How and when do Pt- and Pd-semimetal minerals crystallize from saturated sulfide liquids?

Hassan M. Helmy[1]*, Roman Botcharnikov[2], Chris Ballhaus[3] and Stephan Buhre[2]

[1]Department of Geology, Minia University, Minia, Egypt, [2]Institut Fur Geowissenschaften, Gutenberg Universitat Mainz, Mainz, Germany, [3]Steinmann Institut, Universitat Bonn, Bonn, Germany

Platinum and Pd-arsenides, antimonides, tellurides, bismuthinides, and sulfides are the major hosts of Pt and Pd in magmatic and hydrothermal Cu-Ni-sulfide ores. Textural relationships among such minerals in nature often provide contradictory messages about the mechanism and timing of their formation. To know how and when Pt and Pd mineral phases crystallize from sulfide-saturated liquids and how their compositions and textures evolve during cooling, we undertook controlled cooling experiments in evacuated silica tubes. A Cu-Ni-Fe sulfide mixture, similar in composition to the average Merensky Reef sulfide magma, was charged (in a 9:1 wt.% proportion) with one of the $PtAs_2$, $PtTe_2$, $PtSb_2$, $PtBi_2$, $PdAs_2$, $PdTe_2$, PdSb, and $PdBi_2$ compounds, heated to 1,100°C, and slowly cooled (15°C/day) to room temperature. The run products were sampled at 950°C, 750°C, and 25°C by quenching the silica tubes in water. The results show that Pt formed stable phases with As, Te, and Sb above 950°C and with Bi and S below 750°C. The Pt phases were found mostly in the decomposed intermediate solid solution (ISS), and all the phases survived to 25°C with no compositional changes. At 950°C, Pd formed arsenide, telluride, and antimonide immiscible melts that coexisted with monosulfide solid solution (MSS) and sulfide melt. The composition of the Pd-semimetal melt droplets changed during cooling by equilibration with the host sulfide. Palladium mineral phases formed at temperatures below 750°C directly from the immiscible semimetal-rich melts where they kept the rounded shapes of the melt droplets. Ni-sulfarsenides preceded the formation of Pd arsenides. No Ni tellurides, antimonides, or bismuthinides formed in any of the systems, implying that their formation requires higher semimetal/Pt + Pd ratios. The decomposition of MSS and ISS to base metal sulfides led to significant textural changes in Pt and Pd mineral grains. The compositions of Pt and Pd phases are inherited from the magmatic stage, and their textures are low-temperature (<450°C) features.

KEYWORDS

Platinum-group minerals, platinum, palladium, semimetals, magmatic sulfide deposits

1 Introduction

Platinum and Pd are present in magmatic sulfide deposits mainly as platinum-group minerals (Daltry and Wilson, 1997; Cabri and Laflamme, 1976; Magyarosi et al., 2002; Cawthorn, 2002; Barkov et al., 2002; McDonald, 2008; Godel et al., 2007; Dare et al., 2010 and many others). Common Pt- and Pd-minerals include arsenides (sperrylite, $PtAs_2$, palladoarsenide, and $PdAs_2$), tellurides (moncheite $PtTe_2$ and merenskyite PdTe),

antimonides (geversite $PtSb_2$ and sudburyite PdSb), and bismuthinides (insizwaite $PtBi_2$ and froodite $PdBi_2$). Because these minerals are commonly associated with base-metal sulfides (BMS) in nature, they are thought to form by solid-state exsolution from sulfide minerals (Ballhaus and Ryan, 1995; Prichard et al., 2004; Godel et al., 2007) or crystallize directly from magmatic melts (Hanley, 2007; Helmy et al., 2007; 2013; 2023; Holwell and McDonald, 2007; Godel et al., 2010; Junge et al., 2014; Maier et al., 2015; Barnes et al., 2016). As natural sulfides hardly preserve original magmatic textures during cooling, it is very challenging to use textures of natural Cu-Ni-sulfide ores for the reconstruction of sulfide evolution processes. In particular, crystallization kinetics and the compositional and textural evolution of Pt and Pd mineral phases during cooling from magmatic to room temperatures remain poorly understood.

Many experimental studies on the behavior of Pt and Pd in sulfide systems have been conducted during the last 2 decades, covering the temperature range of magmatic deposits, i.e., from 1,150°C–750°C (Helmy et al., 2007; 2013; Bai et al., 2017; Helmy and Bragagni, 2017; Helmy and Fonseca, 2017; Helmy and Botcharnikov, 2020; Piña et al., 2020). In these studies, Pt- and Pd-semimetal saturated sulfide systems were equilibrated at fixed temperatures. Owing to the restricted temperature range, the previous studies did not show when and how the Pd-semimetal minerals form or how the Pt and Pd mineral compositions and textures evolve during cooling, resulting in the understanding of the genesis of magmatic sulfide deposits and behavior of metals in metallurgical purposes remaining elusive.

In the present study, we used a progressive stepped experimental approach to investigate the evolution of Pt- and Pd-semimetal saturated sulfide melts during slow cooling (15°C/day) from a magmatic temperature (1,100°C) to room temperature. This approach allows the monitoring of the textural evolution and compositional variations of Pt- and Pd mineral phases. We added the Pt-semimetal ($PtAs_2$, $PtTe_2$, $PtSb_2$, and $PtBi_2$) and Pd-semimetal ($PdAs_2$, $PdTe_2$, PdSb, and $PdBi_2$) compounds to a mixture of basic sulfide metals [$(FeNiCu)_{0.99}S_{1.0}$].

1.1 Previous experimental studies

Previous experimental studies (Helmy et al., 2007; 2013; Helmy and Bragagni, 2017; Helmy and Fonseca, 2017; Helmy and Botcharnikov, 2020; Pina et al., 2020; Helmy et al., 2023) described the stable Pt and Pd phases at magmatic temperatures and showed how Pt and Pd partition between MSS and sulfide melts. Some of the Pt- and Pd-semimetal mineral phases were not reported in these studies because they likely form only at lower temperatures. In the arsenide-saturated systems (Helmy et al., 2013), sperrylite is stable above 950°C in the $PtAs_2$-saturated system, while no Pd-arsenides are stable above 750°C in the $PdAs_2$-saturated system. Palladium forms immiscible Pd-arsenide melt down to 750°C. High concentrations (>1,100 ppm) of Pd and As are detected in MSS at 950°C. In the $PtTe_2$- and $PdTe_2$-saturated systems, moncheite ($PtTe_2$) is stable above 950°C in the $PtTe_2$-saturated system, while no Pd-tellurides are stable above 750°C (Helmy et al., 2007). The MSS accommodates approximately 0.2 wt.% of Pt, Pd, and Te at 920°C. In the Sb-PGM-saturated systems (Helmy and

Botcharnikov, 2020), geversite ($PtSb_2$) forms euhedral crystals in MSS at 950°C in the $PtSb_2$-saturated sulfide system while no Pd-antimonide phases form down to 750°C in the PdSb-saturated sulfide system. Platinum contents in MSS in the Sb-PGM-saturated systems are approximately 0.1 wt.%, and Pd and Sb contents in MSS are below the Electron Probe Micro Analyzer (EPMA) detection limit (0.04 wt.%) at 950°C. In the Bi-PGM-saturated systems (Helmy and Botcahrnikov, 2020), insizwaite ($PtBi_2$) and froodite ($PdBi_2$) are stable at 780°C and 750°C, respectively. Although MSS accommodates >0.2 wt.% Pt and Bi, the Pd content is close to the EPMA detection limit. The sulfide melts of all systems accommodate wt.% levels of Pt, Pd, and the semimetals (Helmy et al., 2007; 2013; Helmy and Bragagni, 2017; Helmy and Botcahrnikov, 2020; Pina et al., 2020).

1.2 Experimental and analytical techniques

A sulfide mixture (Cu 7.8 wt%., Ni 16 wt.%, Fe 40.2 wt.%, and S 36 wt%) similar in composition to the average composition of the Merensky Reef sulfides was mixed with Pt-arsenide, ($PtAs_2$) antimonide ($PtSb_2$), telluride ($PtTe_2$), and bismuthinide ($PtBi_2$) mineral phases and Pd-arsenide ($PdAs_2$), antimonide (PdSb), telluride ($PdTe_2$), and bismuthinide ($PdBi_2$) mineral phases. The sulfide and Pt- and Pd-ligand components were synthesized separately from Pt and Pd powders and elemental S, Ni, Fe, Cu, Te, As, Sb, and Bi. The nine starting components, $(FeCuNi)_{0.99}S_{1.0}$, $PtTe_2$, $PtSb_2$, $PtAs_2$, $PtBi_2$, $PdTe_2$, PdSb, $PdAs_2$, and $PdBi_2$, were charged individually in SiO_2 glass tubes, which were evacuated to an approximate pressure of 1 Pa pressure and welded shut. The tubes were heated stepwise from 90°C to 700°C overnight (for the sulfide component) and to 1,250°C (for the Pt- and Pd-semimetal components) until all metals and elemental S, Te, As, Sb, Bi, and Se were consumed.

After regrounding the pre-reacted mixtures, three charges were prepared from each mixture, in which 165 mg aliquots (approximately 150 mg of the sulfide component and 15 mg of either $PtTe_2$, $PtSb_2$, $PtAs_2$, $PtBi_2$, $PdTe_2$, PdSb, $PdAs_2$, or $PdBi_2$) were welded in evacuated SiO_2 glass tubes. The capsules were then reacted in a normal furnace to 1,150°C and slowly cooled (15°C/day) to the desired temperature. The pS_2 was not controlled but when crystalline MSS is in a stable phase, pS_2 can be estimated from the mole fraction of FeS in $(Fe, Ni)_{1-x}S$ solid solutions (cf. Toulmin and Barton, 1964; Barin 1995; Helmy et al., 2010).

The first set of charges (one of each mixture) was quenched at 950°C, the second at 750°C, and the last was cooled to room temperature (25°C). Quenching of the experiments was achieved by removing the capsules from the furnace and dropping them in cold water. The run products were then mounted in epoxy, grounded, and polished for microscope examination and electron microprobe analysis.

1.3 Analytical details

Sulfide and platinum-group mineral phases were analyzed for major elements (S, Fe, Cu, Ni, Pt, Pd, Te, and Sb) using a JEOL JXA

TABLE 1 Phase compositions of the Pt-saturated systems at 950, 750 and 25°C.

PtAs2-saturated experiments

Run Temp.	950°C			750°C			25°C				
Phase	MSS	SM	Spr	MSS	SM	Spr	Po	Ccp	Granular Pn	Spr	Coop
S	37.57 ± 0.33	29.61 ± 1.03	0.17 ± 0.13	37.86 ± 0.29	33.61 ± 0.59	0.89 ± 0.15	37.98±0.34	35.75 ± 0.27	34.93 ± 0.28	0.45 ± 0.33	15.37 ± 1.09
Fe	42.24 ± .94	20.65 ± 1.81	0.24 ± 0.11	40.00 ± 0.24	32.20 ± 0.68	0.11 ± 0.07	38.19±0.77	38.92 ± 1.49	29.21 ± 0.48	0.04 ± 0.04	1.08 ± 1.61
Ni	14.93 ± 0.63	17.20±3.69	0.15 ± 0.12	18.39 ± 0.33	4.87±0.28	0.12 ± 0.09	20.76 ± 0.69	2.54 ± 0.35	35.32 ± 0.39	0.04 ± 0.04	0.83 ± 0.07
Cu	2.37 ± 0.19	22.68 ± 7.06	0.07 ± 0.03	2.70 ± 0.14	26.98 ± 0.55	0.02 ± 0.03		20.79 ± 1.90		0.04 ± 0.06	0.93 ± 1.17
Pt	0.41 ± 0.24	4.58 ± 1.24	56.21 ± 1.51	0.33 ± 0.36	0.47±0.62	55.24 ± 0.57	0.34 ± 0.33	0.39 ± 0.33	0.45 ± 0.35	57.70 ± 1.09	80.83 ± 3.84
As	0.12 ± 0.04	3.69 ± 0.84	41.80 ± 1.34	0.01 ± 0.01	0.30 ± 0.70	41.87 ± 0.29	0.02 ± 0.01	0.01 ± 0.01	0.02 ± 0.02	40.55 ± 0.88	0.02 ± 0.02
Total	97.62 ± 0.82	98.41 ± 0.51	98.64 ± 0.98	99.29 ± 0.33	98.43 ± 0.62	98.24 ± 0.60	97.29 ± 0.86	98.40 ± 0.38	99.93 ± 0.52	98.80 ± 1.22	99.04 ± 0.70
Metal/S	0.889 ± 0.012	1.105 ± 0.052		0.903 ± 0.008	1.033 ± 0.007		0.869 ± 0.006	0.954 ± 0.009	1.044 ± 0.014		

PtTe2-saturated experiments

Phase	MSS	SM	Mon	MSS	SM	Mon	Po	Ccp	Pn	Mon
S	37.87 ± 0.48	29.61 ± 1.03	0.20 ± 0.04	37.96 ± 0.36	33.94 ± 0.25	0.16 ± 0.02	38.51 ± 0.33	36.06 ± 0.46	33.04 ± 0.13	0.21 ± 0.03
Fe	41.84 ± 1.08	20.65 ± 1.81	0.04 ± 0.04	39.76 ± 0.34	31.69 ± 0.41	0.02 ± 0.02	38.95 ± 0.48	38.66 ± 1.05	28.21 ± 0.39	0.04 ± 0.04
Ni	15.83 ± 0.78	17.20 ± 3.69	0.15 ± 0.02	17.94 ± 0.21	5.11 ± 0.36		21.76 ± 0.48	2.97 ± 0.62	36.81 ± 0.22	0.04 ± 0.05
Cu	2.78 ± 0.23	22.68 ± 7.06	0.12 ± 0.21	2.63 ± 0.08	27.84 ± 0.23			19.87 ± 1.10		
Pt	0.61 ± 0.38	4.58 ± 1.24	41.27 ± 0.78	0.68 ± 0.51	0.61 ± 0.29	41.98 ± 0.45	0.44 ± 0.36	0.66 ± 0.46	0.41 ± 0.43	41.61 ± 1.26
Te	0.22 ± 0.04	3.69 ± 0.84	56.68 ± 0.37	0.06 ± 0.03	0.07 ± 0.04	56.81 ± 0.27	0.10 ± 0.04	0.04 ± 0.04	0.11 ± 0.04	56.37 ± 0.33
Total	99.13 ± 0.96	98.41 ± 0.51	98.46 ± 1.016	99.03 ± 0.68	99.26 ± 0.59	98.96 ± 0.57	99.75 ± 0.65	98.26 ± 1.06	98.59 ± 0.88	98.26 ± 1.41
metal/S	0.889 ± 0.012	1.105 ± 0.052		0.885	1.025 ± 0.011					

PtSb2-saturated experiments

Phase	MSS	SM	Gev	MSS	SM	Gev	Po	Ccp	Pn	Gev
S	38.02 ± 0.43	31.50 ± 2.07	0.19 ± 0.01	38.99 ± 0.21	34.68 ± 0.24	0.29 ± 0.01	39.38 ± 0.49	37.02 ± 0.66	35.01 ± 0.42	0.26 ± 0.06
Fe	43.02 ± 0.42	25.17 ± 6.31	0.06	38.95 ± 0.47	31.35 ± 1.23		38.18 ± 0.82	37.80 ± 2.15	28.61 ± 0.26	
Ni	14.30 ± 0.44	14.50 ± 3.92	0.11	17.64 ± 0.28	5.05 ± 0.29		20.92 ± 0.54	2.48 ± 0.57	35.89 ± 0.33	0.05 ± 0.03
Cu	2.60 ± 0.06	17.44 ± 12.00	0.12 ± 0.06	2.75 ± 0.08	27.03 ± 0.92	0.06 ± 0.06		20.45 ± 2.53		0.06 ± 0.06
Pt	0.55 ± 0.39	3.90 ± 1.86	45.18 ± 2.11	0.60 ± 0.40	0.52 ± 0.41	44.88 ± 1.09	0.36 ± 0.41	0.46 ± 0.41	0.46 ± 0.36	43.00 ± 0.85
Sb	BDL	6.04 ± 1.07	53.25 ± 1.05	BDL	0.03 ± 0.02	53.65 ± 0.24				52.60 ± 0.37

TABLE 1 (*Continued*) Phase compositions of the Pt-saturated systems at 950, 750 and 25°C.

PtSb2-saturated experiments									
Phase	MSS	SM	Gev	MSS	SM	Gev	Po	Ccp	Pn	Gev
Total	98.53 ± 0.98	98.55 ± 1.08	98.91 ± 1.32	98.93 ± 0.31	98.66 ± 1.79	98.88 ± 1.32	98.83 ± 1.35	98.21 ± 0.91	99.98 ± 0.82	98.91 ± 1.07
Metal/S	0.889540979485942	0.991054724927232		0.865072400908884	1.00362175482741					

PtSBi2-saturated experiments									
Phase	MSS	SM	MSS	SM	Pt-bismuthinide Melt	Po	Ccp	Pn	Cb	Ins
S	37.04 ± 0.11	35.78 ± 1.17	38.39 ± 0.33	34.11 ± 0.42	5.67 ± 1.49	38.54 ± 0.34	35.81 ± 0.38	33.55 ± 0.24	36.01 ± 0.29	0.56 ± 0.88
Fe	44.18 ± 0.18	27.00 ± 4.73	40.91 ± 0.41	30.85 ± 0.51	0.26 ± 0.13	45.01 ± 1.17	35.71 ± 2.48	28.90 ± 0.73	40.48 ± 0.36	1.00 ± 0.97
Ni	13.78 ± 0.39	23.56 ± 4.78	16.09 ± 0.14	5.92 ± 0.56	2.62 ± 1.21	14.61 ± 1.25	1.55 ± 0.61	35.85 ± 0.48	2.81 ± 0.16	0.14 ± 0.08
Cu	2.30 ± 0.11	9.80 ± 6.71	2.51 ± 0.10	27.04 ± 0.79	2.32 ± 1.14		25.83 ± 3.40		18.96 ± 0.45	0.56 ± 0.44
Pt	0.59 ± 0.32	0.92 ± 0.46	0.60 ± 0.35	0.52 ± 0.41	27.75 ± 3.48	0.44 ± 0.31	0.59 ± 0.42	0.50 ± 0.36	0.54 ± 0.23	31.88 ± 2.41
Bi	0.18 ± 0.05	1.04 ± 0.69	0.18 ± 0.04	0.23 ± 0.06	59.42 ± 2.83	0.20 ± 0.04	0.18 ± 0.03	0.12 ± 0.05	0.15 ± 0.05	63.45 ± 1.50
Total	98.08 ± 0.51	98.11 ± 0.91	98.68 ± 0.85	98.67 ± 0.82	98.03 ± 1.67	98.79 ± 0.76	99.66 ± 0.78	98.92 ± 1.03	98.96 ± 0.58	97.62 ± 2.42
Metal/S	0.919 ± 0.006	0.959 ± 0.038	0.890 ± 0.006	1.027 ± 0.017	0.475 ± 0.084	0.886 ± 0.012	0.966 ± 0.024	1.084 ± 0.009	0.950 ± 0.009	

* MSS monosulfide solid solution, SM sulfide melt, Spr sperylite, Po pyrrhotite, Ccp chalcopyrite, Cb cubanite, monch moncheite, Pn pentlandite, Mer merenskyite, Sud sudburyite, Fr froodite Gev geversite, Ins insizwite

2 Results

2.1 Phase relations and compositions

In all systems, MSS coexisted with a sulfide melt and a Pt-phase in the Pt-saturated systems or with a Pd-semimetal melt in the Pd-saturated systems at 950°C and 750°C. In the 25°C experiments, MSS exsolved pentlandite in a matrix of Ni-rich pyrrhotite, while ISS exsolved chalcopyrite, cubanite (a Ccp-Cb matrix), and pentlandite. Tables 1, 2 list the average compositions of sulfide and Pt- and Pd-mineral phases in all systems. Apart from Pt sulfide and the bismuthinide phases, all Pt mineral phases were high-temperature phases formed above 950°C and persisted to 25°C with no significant change in composition. Although Pt phases of the 950°C experiments formed inclusions in MSS, they were preserved as interstitial grains in the decomposed MSS at 25°C.

825 electron microanalyzer operated at 15 kV and 20 nA. All phases were analyzed in spot mode, but MSS and the sulfide melt were analyzed with a beam defocused to 30 μm. Standards used were natural Canyon Diablo troilite, metallic Ni, Cu, Pt, Pd, Te, Bi, Sb, and GaAs. For further analytical details see Helmy et al. (2021).

2.2 Platinum-saturated sulfide systems

2.2.1 The PtAs$_2$-saturated system

Sperrylite (PtAs$_2$) formed small euhedral crystals in the 950°C experiment and persisted to 25°C (Figure 1A). Sperrylite in the 750°C experiment was common in the outer rims of MSS (Figure 1B). The sperrylite grain sizes increased, particularly those in the sulfide melt. All sperrylite grains in the 25°C experiments were found at the margins of large MSS masses, where granular pentlandite formed (Figure 1C). In addition to the large euhedral sperrylite, large euhedral cooperite (PtS) crystals developed in the Ccp-Cb matrix of the 25°C experiment (Figure 1D). The PtS crystals did not appear in the 950°C and 750°C experiments. No Ni arsenide phases were found.

The metal/S ratio of MSS at 950°C and 750°C (Table 1) ranged between 0.87 and 0.91, reflecting a range of log fS$_2$ between 1 and −1 (Helmy et al., 2010). Platinum concentrations in MSS were less than 0.4 wt.% in the two experiments. The As contents of MSS in the 950°C and 750°C experiments were below the EPMA detection limit. The As and Pt contents of the sulfide melt of the 750°C experiment were lower than those in the 950°C experiment, suggesting better separation of the immiscible arsenide melt from the sulfide melt. The chemical composition of sperrylite was almost identical at the three investigated temperatures. Cooperite contained approximately 1 wt.% Fe, Cu, and Ni.

TABLE 2 Phase composition of the Pd-saturated systems at 950, 750 and 25°C*.

PdAs2-saturated system											
Run Temp.	950°C			750°C				25°C			
Phase wt.%	MSS	SM	Pd-arsenide melt	MSS	SM	Grs	Pd-arsenide melt	Po	Cb	Pal	Pn
S	38.10 ± 0.30	26.84 ± 2.01	2.54 ± 0.88	37.69 ± 0.28	34.47 ± 0.34	14.70 ± 0.18	0.05 ± 0.03	37.91 ± 0.24	35.74 ± 0.41		32.96 ± 0.19
Fe	44.38 ± 0.39	15.52 ± 2.92	0.21 ± 0.05	40.38 ± 0.29	34.46 ± 0.43	1.64 ± 0.07	0.11 ± 0.06	40.74 ± 0.41	37.72 ± 3.01	0.08 ± 0.02	28.90 ± 0.58
Ni	14.19 ± 0.28	12.95 ± 5.78	11.22 ± 1.96	16.60 ± 0.13	4.27 ± 0.26	24.53 ± 0.63	6.12 ± 1.23	19.81 ± 0.21	2.44 ± 0.92	6.50 ± 0.38	36.39 ± 0.71
Cu	3.00 ± 0.07	26.34 ± 9.21	1.05 ± 0.69	3.17 ± 0.25	25.56 ± 0.28		1.14 ± 0.44		23.54 ± 4.37	0.07 ± 0.04	
Pd	0.17 ± 0.03	2.60 ± 2.81	39.19 ± 5.72	0.08 ± 0.02		11.98 ± 0.93	59.38 ± 2.22			66.54 ± 0.72	
As	0.14 ± 0.03	13.47 ± 3.61	45.04 ± 4.23	0.20 ± 0.02		47.83 ± 0.32	32.88 ± 3.18			26.20 ± 0.34	0.06 ± 0.02
Total	99.96 ± 0.48	97.72 ± 1.21	99.24 ± 0.95	98.11 ± 0.79	98.76 ± 0.69	100.68 ± 0.44	99.69	98.46 ± 0.79	99.44 ± 0.33	99.39 ± 0.59	98.30 ± 1.01
Metal/S	0.906240927153375	1.09151507994907		0.910180269420014	1.02886985151513			0.902767900189469	0.958114772084406		
PdTe2-saturated system											
Phase	MSS	SM	Pd-telluride melt	MSS	SM	Pd-telluride melt	Po	Cb	Mer	Pn	
S	38.95 ± 0.25	32.43 ± 0.39	2.08 ± 1.55	38.52 ± 0.18	34.90 ± 0.36	0.45 ± 0.08	38.41 ± 0.21	36.75 ± 0.23	0.22 ± 0.13	33.74 ± 0.39	
Fe	41.75 ± 1.13	21.58 ± 1.78	0.79 ± 1.21	39.96 ± 0.41	33.03 ± 0.45	0.05 ± 0.03	41.34 ± 0.33	38.98 ± 0.77	0.41 ± 0.19	28.83 ± 0.81	
Ni	14.74 ± 0.94	19.08 ± 4.41	5.29 ± 1.67	17.21 ± 0.32	4.83 ± 0.51	2.78 ± 0.22	19.91 ± 0.19	2.75 ± 0.45	2.45 ± 0.58	36.45 ± 1.23	
Cu	2.90 ± 0.16	19.22 ± 8.71	3.92 ± 0.78	2.73 ± 0.16	25.60 ± 0.29	2.19 ± 0.58		19.65 ± 0.96	0.07 ± 0.08		
Pd	0.35 ± 0.04	2.01 ± 1.04	28.48 ± 2.25	0.06 ± 0.02		31.49 ± 0.39			34.50 ± 5.21		
Te	0.21 ± 0.04	4.71 ± 2.12	59.61 ± 2.67	0.24 ± 0.06	0.24 ± 0.08	64.21 ± 0.66		0.11 ± 0.04	63.36 ± 4.82	0.18 ± 0.06	

(Continued on following page)

TABLE 2 (*Continued*) Phase composition of the Pd-saturated systems at 950, 750 and 25°C*.

PdTe2-saturated system

Phase	MSS	SM	Pd-telluride melt	MSS	SM	Pd-telluride melt	Po	Cb	Mer	Pn
Total	98.91 ± 0.54	99.02 ± 1.36	100.16 ± 1.07	98.71 ± 0.38	98.60 ± 0.68	101.18 ± 0.98	99.66 ± 0.79	98.24 ± 0.84	101.01 ± 0.68	99.19 ± 0.86
metal/S	0.865	0.012		0.886 ± 0.007	1.001 ± 0.008		0.902767900189469	0.942 ± 0.012		1.081 ± 0.017

PdSb-saturated system

Phase	MSS	SM	Pd-antimonide melt	MSS	SM	Pd-antimon. melt	Po	Cb	Sud	Pn
S	38.60 ± 0.30	27.86 ± 1.8	0.27 ± 0.08	38.05 ± 0.31	35.02 ± 0.21	0.01 ± 0.02	38.86 ± 0.34	36.39 ± 0.22	0.03 ± 0.02	34.35 ± 0.79
Fe	44.13 ± 0.29	14.22 ± 3.84	0.10 ± 0.07	40.83 ± 0.51	32.27 ± 0.40	0.05 ± 0.04	39.97 ± 0.48	38.96 ± 1.39	0.12 ± 0.24	29.69 ± 0.83
Ni	13.90 ± 0.22	10.88 ± 6.41	1.82 ± 0.17	16.84 ± 0.18	5.47 ± 0.35	6.14 ± 0.32	19.72 ± 0.37	2.27 ± 0.56	5.65 ± 2.15	34.94 ± 1.28
Cu	2.17 ± 0.16	23.71 ± 9.72	0.84 ± 0.18	2.72 ± 0.33	26.61 ± 0.52	0.06 ± 0.07		21.08 ± 2.05		
Pd	0.09 ± 0.02	1.15 ± 2.44	45.96 ± 1.53			37.45 ± 0.42			38.05 ± 2.82	
Sb		20.38 ± 3.19	49.91 ± 0.59		0.12 ± 0.06	54.73 ± 0.37			54.52 ± 0.79	
Total	98.90 ± 0.63	98.20 ± 0.69	98.91 ± 1.28	98.43 ± 0.41	99.49 ± 0.62	98.44 ± 0.31	98.55 ± 0.57	98.70 ± 0.51	98.37 ± 0.43	98.97 ± 0.47
metal/S	0.884 ± 0.007	0.930 ± 0.035		0.899 ± 0.005	1.030 ± 0.020		0.875 ± 0.009			

PdBi2-saturated system

Phase	MSS	SM	MSS	SM	Pd-bismuth. melt	Po	Cb	Fr	Pn
S	37.86 ± 0.32	31.57 ± 3.81	37.95 ± 0.19	34.90 ± 0.19	4.71 ± 4.87	38.31 ± 0.25	35.99 ± 0.25	0.02 ± 0.01	33.65 ± 0.30
Fe	44.97 ± 0.51	22.11 ± 4.06	39.79 ± 0.33	33.49 ± 0.43	5.41 ± 5.08	38.97 ± 0.81	38.92 ± 1.25	0.02 ± 0.02	28.14 ± 0.36
Ni	13.16 ± 0.34	17.60 ± 5.99	17.95 ± 0.31	5.26 ± 0.49	1.91 ± 2.60	20.91 ± 1.09	2.61 ± 0.59	0.04 ± 0.04	37.68 ± 0.75
Cu	2.22 ± 0.12	15.69 ± 6.23	2.40 ± 0.11	24.92 ± 0.45	2.79 ± 3.25		20.47 ± 1.79	0.01 ± 0.02	0.04 ± 0.12
Pd	0.22 ± 0.04	1.63 ± 1.39	0.12 ± 0.04	0.04 ± 0.02	20.03 ± 3.04	BDL	BDL	19.19 ± 0.11	0.02 ± 0.02
Bi	0.19 ± 0.04	9.76 ± 7.94	0.17 ± 0.06	0.17 ± 0.03	63.50 ± 11.10	0.19 ± 0.03	0.19 ± 0.10	80.88 ± 0.82	0.12 ± 0.06
Total	98.62 ± 0.61	98.35 ± 1.36	98.38 ± 0.67	98.79 ± 0.33	98.34 ± 0.85	98.38 ± 0.71	98.18 ± 0.49	100.17 ± 0.86	99.65 ± 0.60
Metal/S	0.914780584433615	0.985898557891868	0.884 ± 0.007	1.001		0.877 ± 0.009			

* MSS monosulfide solid solution, SM sulfide melt, Grs gersdorfite, Po pyrrhotite, Cb cubanite, Pal palladoarsenide, Pn pentlandite, Mer merenskyite, Sud sudburyite, Fr froodite
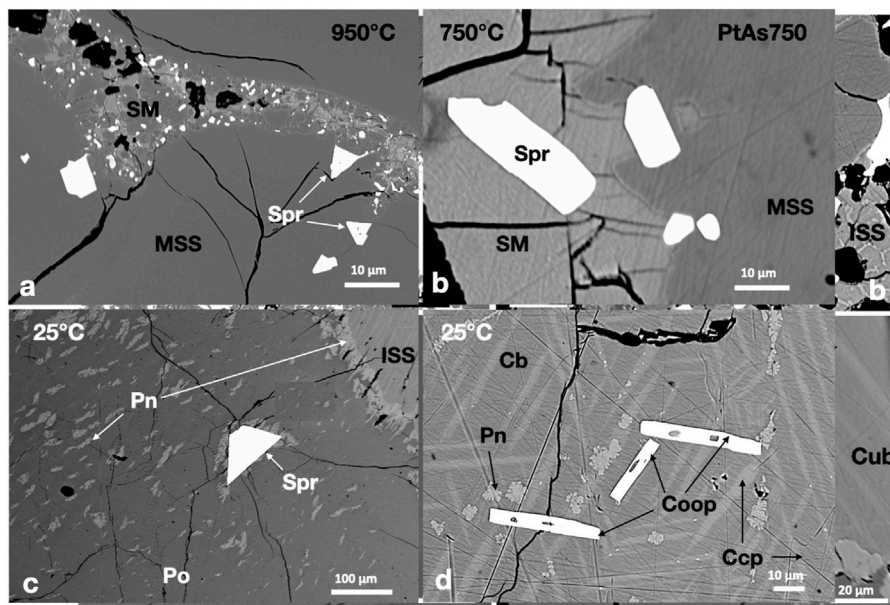
FIGURE 1
Back scatter electron (BSE) images of the phase relations in the PtAs$_2$-saturated experiments. Run temperatures are indicated on the images. **(A)** Euhedral sperrylite (Spr) crystals in the MSS and SM; note the tiny sperrylite crystals in the SM. **(B)** Sperrylite crystals concentrated at the MSS-sulfide melt interface; note their larger size when included in the sulfide melt. **(C)** A large euhedral sperrylite crystal in Ni-rich pyrrhotite (Po); note the pentlandite (Pn) flames around the sperrylite. **(D)** Columnar cooperite crystals in decomposed ISS; ISS exsolves chalcopyrite (Ccp) skeletons and Pn brushes in cubanite (Cb).
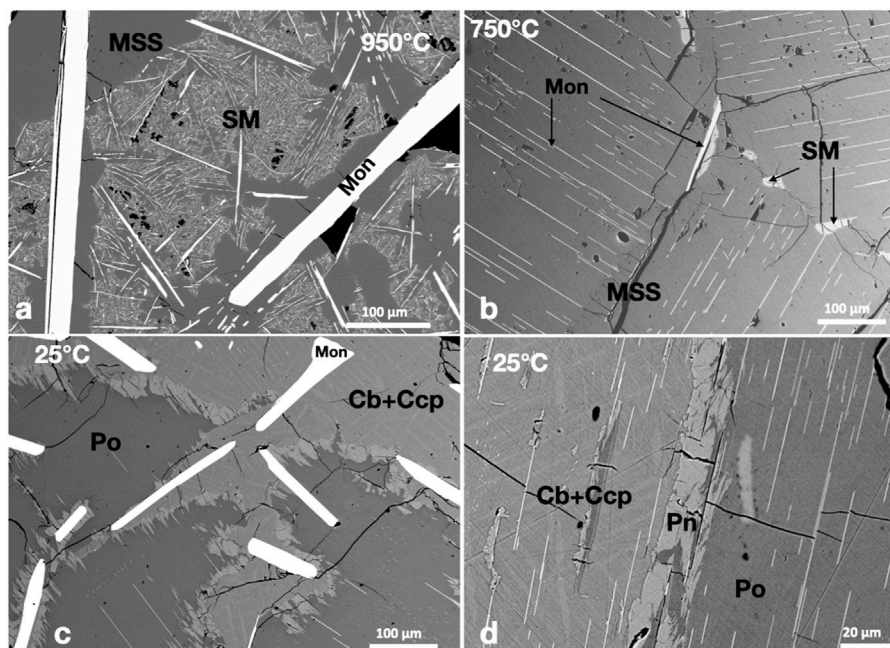
FIGURE 2
BSE images of the phase relations in the PtTe$_2$-saturated experiments. Run temperatures are indicated on the images. **(A)** Large columnar moncheite (Mon) crystals in the MSS and SM. Note the very small needle-like moncheite in the SM. **(B)** Needle-like moncheite grains perfectly oriented in the MSS. Note the different directions in side-by-side MSS masses. **(C)** Large randomly oriented moncheite grains in the Ccp-Cb matrix and oriented needle-like moncheite in Po. **(D)** Perfectly oriented needle-like moncheite grains in Po and the Ccp-Cb matrix. Note the parallel directions in both.

2.2.2 The PtTe$_2$-saturated system

Large moncheite (PtTe$_2$) columnar crystals coexisted with MSS and sulfide melt at 950°C (Figure 2A). The moncheite crystals were millimeters in size when included in large MSS masses and formed smaller sizes in the sulfide melt. At 750°C, in addition to the large columnar crystals in the sulfide melt, thin moncheite needles
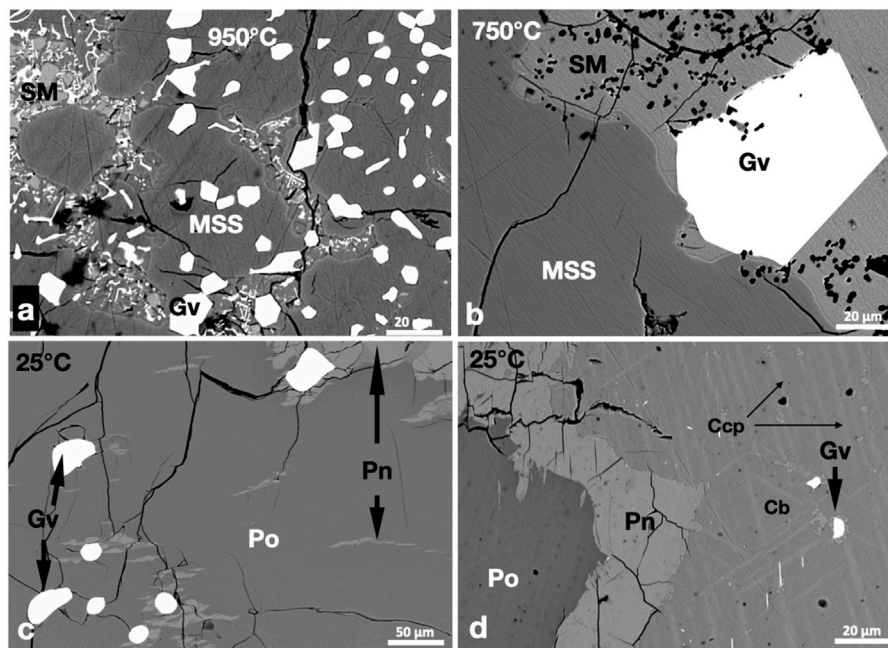
FIGURE 3
BSE images of the phase relations in the PtSb$_2$-saturated experiments. Run temperatures are indicated on the images. **(A,B)** Euhedral geversite (Gv) grains in the MSS and sulfide melt (SM). Note the larger size of geversite in the sulfide melt at 750°C. **(C)** Subhedral geversite grains in Po. Note the flame and granular Pn in and around Po. **(D)** Geversite grains oriented parallel to Ccp skeletons in the Cb matrix. Granular Pn developed at the margins of Po.

appeared perfectly oriented in one direction in the MSS masses. The orientation varied inside the MSS mass (Figure 2B), suggesting that the mass is not a single MSS crystal but made of many individual crystals (e.g., Helmy et al., 2023). In the 25°C experiments, large moncheite needles were present in the Ccp-Cb matrix (Figure 2C). It was interesting to note that moncheite needles also formed in the Ccp-Cb matrix and showed the same orientation as in the adjacent Ni-rich pyrrhotite (Figure 2D). No other Pt phases formed in the telluride-saturated experiment.

The metal/S ratios of MSS in the 950°C and 750°C experiments (Table 1) were very similar (0.89 ± ± 0.01). Additionally, platinum and Te contents in MSS were similar (<0.7 and 0.2 wt.%, respectively). The Pt/Te atomic ratio of MSS was >1.8, suggesting that not all Pt was present as a PtTe component. High Pt and Te contents characterized the sulfide melt in the 950°C experiment, and the Te content in the sulfide melt dropped to <0.04 wt.% at 750°C. Moncheite compositions at the three temperatures were identical, with a slightly Te-rich composition of ($Pt_{0.96}Te_{2.04}$). There was wo difference in composition between the large moncheite needles and thin needles exsolved from MSS and ISS.

2.2.3 The PtSb$_2$-saturated system

Small euhedral geversite (PtSb$_2$) crystals coexisted with MSS and sulfide melt at 950°C. The geversite crystals were either included in masses of MSS or in the sulfide melt (Figure 3A). Geversite grains in the sulfide melt were slightly larger. The sulfide melt was quenched to small metastable MSS grains and ISS. In the 750°C experiment, geversite crystals in the sulfide melt reached large sizes (Figure 3B). Geversite grains originally encapsulated in MSS were commonly surrounded by pentlandite exsolutions at 25°C (Figure 3C). Micron-

sized euhedral grains of geversite were noted in the Ccp-Cb matrix in the 25°C experiment (Figure 3D); they were usually oriented in certain directions and sometimes were associated with pentlandite exsolutions (Figure 3D). No Pt phases other than geversite were noted in the three experiments.

The metal/S ratios of MSS at 950°C and 750°C were in the range of 0.88 to 0.86. As in a previous experimental study (Helmy and Botcahrnikov, 2020), the Sb content of MSS was below the EPMA detection limit (0.03 wt.%). Less than 0.6 wt.% Pt was recorded in MSS at 950°C; the high standard error (0.4 wt.%) reflects the inhomogeneous distribution of Pt in MSS. The Pt content of MSS was approximately 0.5 wt.% at 750°C, suggesting that not all Pt was present as Pt antimonide phases. The Sb and Pt contents of the sulfide melt were high at 950°C but dropped sharply in the 750°C experiment (Table 1). The geversite composition was very similar in the three experiments, with a formula approaching ($Pt_{1.01}Sb_{1.96}$).

2.2.4 The PtBi$_2$-saturated system

A large rounded MSS mass coexisted with Bi-rich sulfide melt at 950°C. The Pt-Bi melt was poorly miscible in the sulfide melt; it wetted MSS grains (Figure 4A). At 750°C, the Pt-Bi melt was separated from the sulfide melt and formed an interconnected melt drainage network between MSS grains (Figure 4B). At 25°C, the Pt-Bi-rich melt crystallized to insizwaite (PtBi$_2$), bismuthinite (Bi$_2$S$_3$), and native bismuth (Figure 4C). The textures suggest that insizwaite crystallized earlier than bismuthinite and native bismuth. Micron-sized euhedral cooperite (PtS) grains grew in the MSS and Ccp-Cm matrix, which was frequently overgrown by pentlandite exsolutions (Figure 4D).
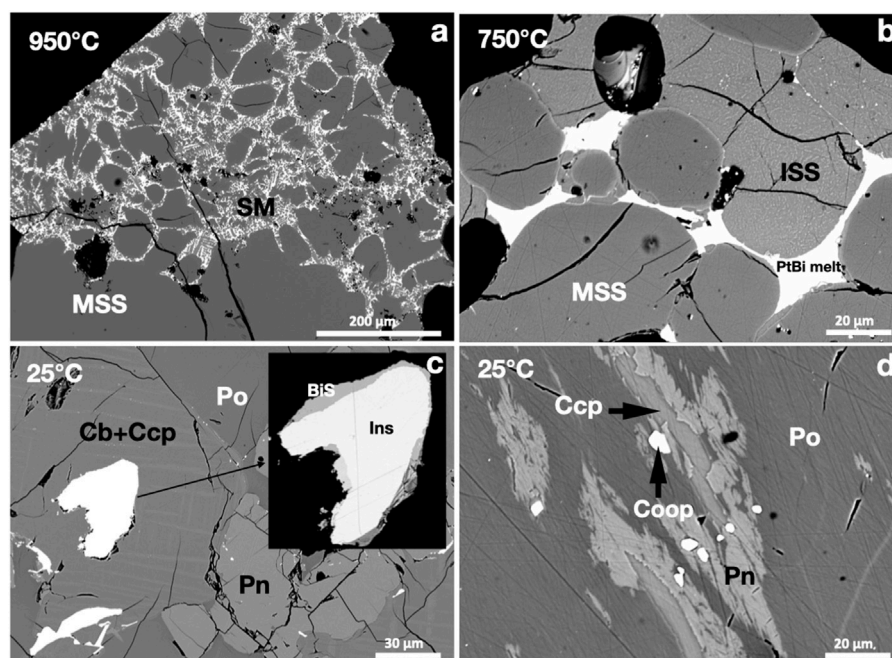
FIGURE 4
BSE images of the phase relations in the PtBi$_2$-saturated experiments. Run temperatures are indicated on the images. **(A)** Bi-rich sulfide melt (SM) and MSS. **(B)** Pt-bismuthinide melt filling between MSS and ISS grains. **(C)** A subhedral Pt-bismuthinide grain in the Ccp-Cb matrix; insizwaite (Ins) and bismuthinite (BiS) crystallized from the bismuthinide melt. **(D)** Subhedral cooperite (Coop) grains in Ccp and Pn exsolutions in Ni-rich Po.
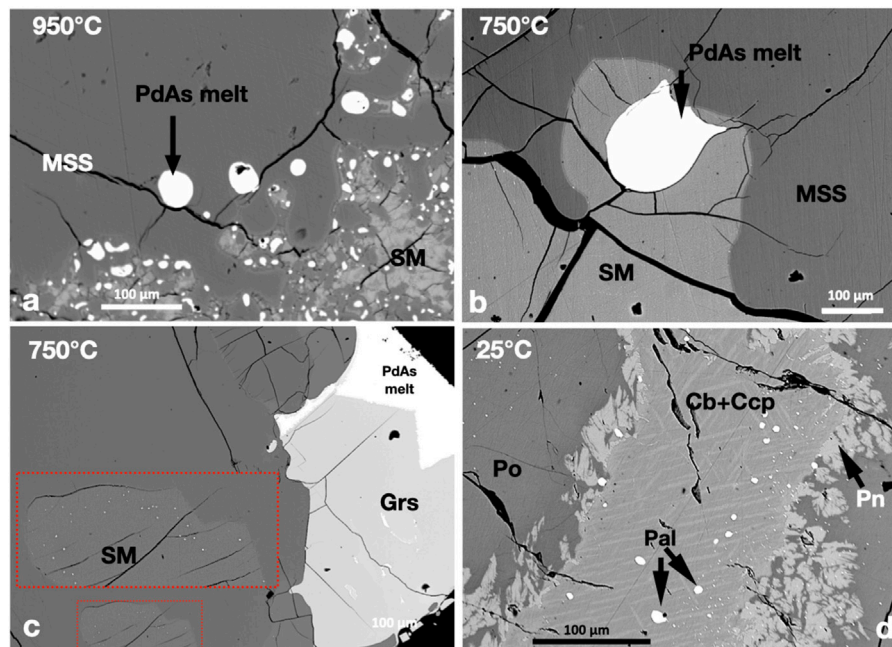
FIGURE 5
BSE images of the phase relations of the PdAs$_2$-saturated experiments. Run temperatures are indicated on the images. **(A,B)** Rounded immiscible Pd-arsenide melt droplets in MSS and SM at 950°C and 750°C, respectively. **(C)** Euhedral gersdorfite crystals growing inside the Pd-arsenide melt droplet. Note the tiny Pd-arsenide melt grains in the fronts of the MSS (inserts). **(D)** Subhedral palladoarsenide (Pal) grains in the Ccp-Cb matrix. Note the tiny Pal grains in the Pn and Po.

The metal/S ratio of the MSS in the 950°C experiment (0.91) was slightly higher than that in the 750°C experiment (0.89). Platinum and Bi contents in the MSS of the 950°C and 750°C experiments were similar, with a Pt/Bi atomic ratio of >2.3, suggesting that Pt was present as other species than PtBi$_2$. The sulfide melt dissolved at approximately 1 wt.% Pt and Bi at 950°C and at approximately
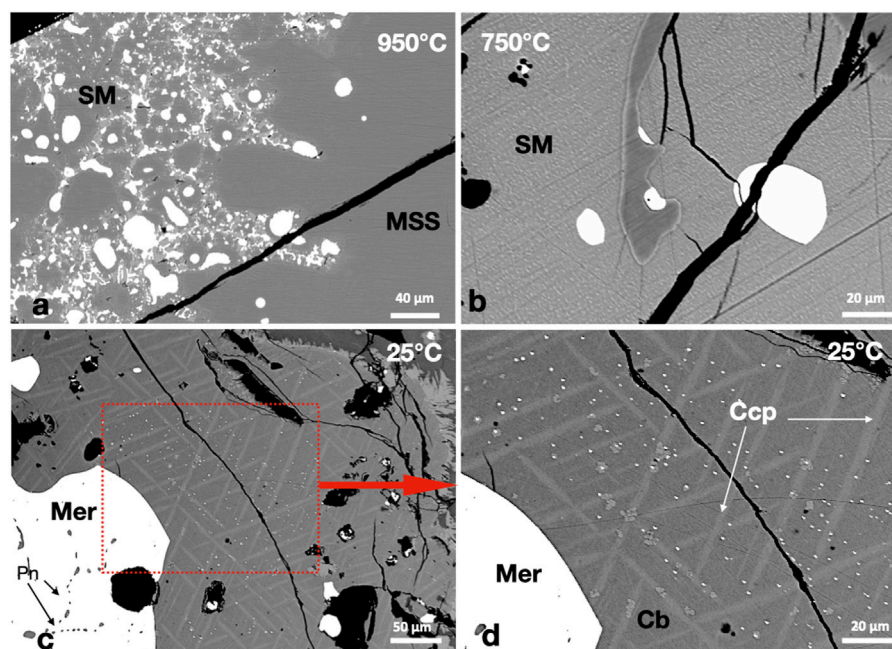
FIGURE 6
(A) A large MSS mass encapsulates rounded Pd-telluride melt droplets (white) and two immiscible melts, Pd-telluride melt and sulfide melt (SM). **(B)** Complete separation between the Pd-telluride melt (white) and the sulfide melt. **(C,D)** A large merenskyite (Mer) mass formed of individual crystals separated by Pn and plenty of micron-sized Mer crystals randomly distributed in the Ccp-Cb matrix.

0.5 wt.% Pt and <0.2 wt.% Bi at 750°C. The Pt/Bi atomic ratios of Bi-rich areas wetting MSS at 950°C, immiscible PtBi melt at 750°C, and insizwaite at 25°C were approximately 0.5 (Table 1). The S, Fe, Ni, and Cu contents of the Pt-bismuthinide melt decreased with falling temperature (Table 1).

2.3 Palladium-saturated sulfide systems

2.3.1 The PdAs$_2$-saturated system

Immiscible Pd-arsenide melt coexisted with sulfide melt and MSS at 950°C (Figure 5A). The Pd-arsenide melt formed rounded droplets in MSS and the sulfide melt. At 750°C, the MSS grains assembled to large MSS masses that trapped continuous sulfide melt areas. Immiscible Pd-arsenide melt formed large droplets in the sulfide melt at 750°C (Figure 5B). Gersdorffite (NiAsS) developed large euhedral crystals in the Pd-arsenide melt globules at 750°C (Figure 5C). The surfaces of gersdorffite crystals against the Pd-arsenide melt were well-developed but not straight against the MSS (Figure 5C). Micron-sized droplets of Pd-arsenide melt were usually present in the sulfide melt in the fronts of MSS grains at 750°C (insert on Figure 5C). At 25°C, in addition to gersdorffite, the Pd-As melt crystallized to palladoarsenide ((PdNi)$_2$As). Additionally, small and tiny palladoarsenide grains were found in the Ccp-Cb matrix and pyrrhotite (Figure 5D).

The metal/S ratios of MSS at 950°C and 750°C were 0.91. The Pd content in MSS was less than 0.2 wt.% at 950°C and dropped to <0.03 wt.% in pyrrhotite at 25°C. The Pd and As contents of the sulfide melt and ISS were below the EMPA detection limit (0.03 wt.%) at 750°C, indicating the complete separation of the Pd

arsenide melt from the sulfide melt. The Ni and S contents of the Pd-arsenide melt decreased when gersdorffite became a stable phase at 750°C. Chalcopyrite and cubanite solid solutions and pentlandite in the 25°C experiment contained Pd and As below the EPMA detection limit.

2.3.2 The PdTe$_2$-saturated system

At 950°C, the MSS coexisted with two immiscible melts: sulfide and Pd-telluride melts (Figure 6A). The immiscible Pd-telluride melt persisted to 750°C; it formed rounded globules in the sulfide melt (Figure 6B). The Pd-telluride melt crystallized to merenskyite (PdTe$_2$) and small pentlandite crystals in the 25°C experiment (Figure 6C). Merenskyite kept the outline of the Pd-telluride melt. In addition to the large merenskyite grains, plenty of micron-sized grains were randomly distributed in the Ccp-Cb matrix, with no preference for chalcopyrite or cubanite (Figures 6C,D). No Ni tellurides were found.

The MSS and sulfide melt in the 950°C experiment accommodated appreciable amounts of Pd and Te (Table 2). The Pd contents of MSS and sulfide melt dropped sharply at 750°C (Table 2). The Pd-telluride melts in the 950°C and 750°C experiments accommodated high S, Cu, Ni, and Fe contents (Table 2). Merenskyite contained high Ni and was usually Te depleted with a formula approaching (PdNi)$_{1.25}$ (TeS)$_{1.75}$. The Ccp-Cb matrix in the 25°C experiment contained Pd and Te contents below the EMPA detection limit.

2.3.3 The PdSb-saturated system

At 950°C, Pd-antimonide melt formed immiscible droplets in sulfide melt; both melts coexisted with MSS (Figure 7A). The Pd-
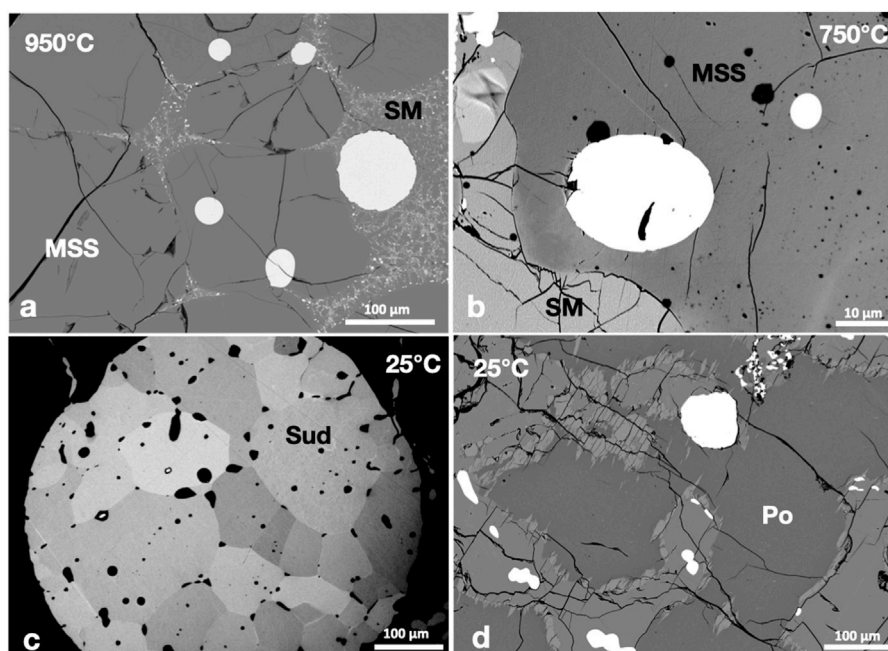
FIGURE 7
(A,B) Rounded immiscible Pd-antimonide melt droplets (white) in MSS and sulfide melt (SM). **(C)** A rounded Pd-antimonide melt droplet hosted in Po crystallized to sudburyite (Sud). Note the well-defined crystal faces of sudburyite against other sudburyite crystals and the rounded faces against Po. **(D)** Small sudburyite grains in the Ccp-Cb matrix.

antimonide melt persisted to 750°C. All the Pd-antimonide melt droplets were large; an almost complete separation of the sulfide and antimonide melts occurred at 750°C. Although the Pd-antimonide globules included in the MSS kept the rounded outline (Figure 7B), they developed small euhedral sudburyite ((PdNi)Sb) crystals at 25°C (Figure 7C). The sudburyite crystals formed a mosaic structure with well-developed crystal surfaces inside the globule but rounded against the MSS (Figure 7C). The small sudburyite grains inside the Ccp-Cb matrix were subhedral to rounded; they were originally concentrated at the MSS-ISS contact (Figure 7D). No Ni-antimonide phases were found.

The Pd and Sb contents of MSS at all temperatures was very low (<0.04 wt.%; Table 2). The large error of the Sb content in the sulfide melt in the 950°C experiment reflected a bad separation of the antimonide and sulfide melts. Palladium and Sb were undetectable in cubanite and chalcopyrite solid solutions and pentlandite in the 25°C experiment.

2.3.4 The PdBi$_2$-saturated system

Like the PtBi$_2$-saturated experiments, the Pd-bismuthinide melt was poorly miscible in the sulfide melt at 950°C. MSS formed a large mass wetted by a thin layer of Pd-bismuthinide melt (Figure 8A). The Bi-rich sulfide melt was quenched to metastable MSS grains in a matrix of Bi-rich melt. At 750°C, the Pd-bismuthinide melt formed interstitial areas between the MSS grains (Figure 8B) or small rounded grains at the MSS-sulfide melt interface (Figure 8C). Froodite (PdBi$_2$) was the only Pd phase in the 25°C experiment; it formed subhedral grains in the Ccp-Cb matrix (Figure 8D).

The Pd and Bi contents of MSS in the 950°C and 750°C experiments were lower than 0.2 wt.% and dropped to <0.03 wt.%

in pyrrhotite at 25°C. Owing to the weak separation of the bismuthinide melt and the sulfide melt at 950°C, the sulfide melt contained high Bi and Pd contents, and the bismuthinide melt contained high S, Fe, Ni, and Fe contents (Table 2). The Pd-content of the sulfide melt at 750°C was below the EPMA detection limit. Froodite was slightly Bi-rich, with an average formula of Pd$_{0.95}$Bi$_{2.05}$. The Pd and Bi contents of the Ccp-Cb matrix in the 25°C experiment were below the EPMA detection limit (0.03 wt.%).

3 Discussion

The experiments were conducted to investigate how and when Pt and Pd semimetal minerals form from saturated sulfide melts and how the textures and compositions of these minerals develop during cooling. The progressive stepped experimental approach allows answering these questions. Knowing when the Pt and Pd mineral phases form is possible by comparing the mineralogy at various temperatures and determining the temperature at which the corresponding Pt- and Pd-semimetal minerals appear. In addition, a comparison of the textures and compositions of phases along the cooling path shows the evolution in each system.

1) How and when do Pt and Pd-semimetal minerals form?

The results of the investigation reveal distinct textural differences between the Pt- and Pd-saturated systems. Consistent with previous experimental studies (Helmy et al., 2007; 2013; Helmy and Bragagni, 2017; Helmy and Fonseca, 2017; Helmy and Botcahrnikov, 2020), Pt forms stable phases with As, Te, and Sb
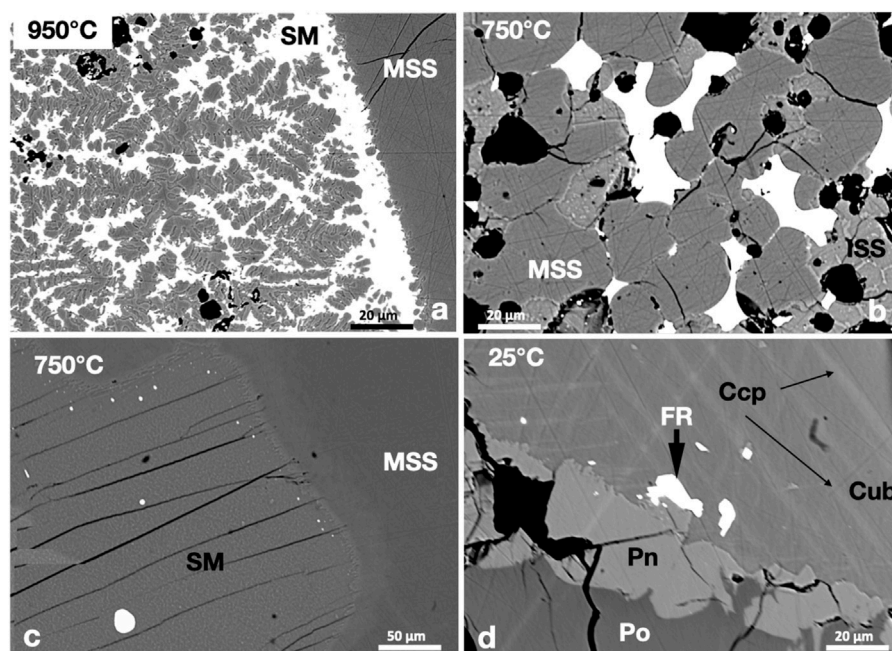
FIGURE 8
(A) Bi-rich sulfide melt (SM, white), metastable MSS (dendritic shape), and stable MSS (the homogenous gray area to the right). **(B)** Pd-bismuthinide melt (white) filling between MSS and ISS grains. **(C)** Small rounded Pd-bismuthinide melt droplets concentrated in the fronts of the MSS. **(D)** Subhedral froodite grains in the Ccp-Cb matrix. Note the tiny froodite grains at the margin of pentlandite.

above 950°C. Cooperite (PtS) appears in the 750°C experiment but insizwaite ($PtBi_2$) is stable only below 750°C. All the high-temperature Pt minerals obtain euhedral outlines, even those included in the MSS; they all likely crystallized before or simultaneously with MSS. The euhedral shape of cooperite hosted in the ISS may suggest that it crystallized from the fractionated sulfide melt above 750°C. Judging from the rounded shape of the insizwaite grains, it seems that it crystallized after the complete solidification of the sulfide melt into ISS.

In the Pt-saturated systems, $PtTe_2$ (moncheite), $PtAs_2$ (sperrylite), and $PtSb_2$ (geversite) are high-temperature phases; they form large euhedral grains in the MSS and sulfide melt at 950°C. It is evident that the large euhedral Pt-semimetal minerals at 950°C crystallized directly from the semimetal-saturated sulfide melt, whereas insizwaite crystallized from the immiscible bismuthinide melt below 750°C. In addition to these large euhedral crystals, the 25°C experiments produce very small sperrylite, geversite and cooperite crystals in the decomposed MSS. The textures suggest that these very small crystals exsolved from the MSS during cooling. Helmy et al. (2023) showed that Pt and the semimetals are hosted in the magmatic MSS as nanoparticles. These small crystals were hosted as sub-micron particles in MSS of the 950°C and assembled to larger sizes on cooling.

Although S is a major component in all the examined systems, the Pt-sulfide phase (cooperite) formed only in the $PtBi_2$-and $PtAs_2$-saturated experiments. The strong Pt-Sb and Pt-Te complexation probably does not leave any Pt free to react with S, while Bi has a weaker affinity with complex Pt (Helmy and Botcahrnikov, 2020), leaving some Pt to combine with S. In addition, As valency is

strongly dependent on the oxidation state of the system (Helmy et al., 2010); an increase in fS_2 forces some As to act as an electron recipient (combines with S), leaving some Pt to be complexed with S to form cooperite. Helmy et al. (2023) showed that Pt is accommodated in the MSS, in addition to the Pt-semimetal nanoparticles, as Pt-sulfide nanoparticles, especially in Bi- and Te-saturated sulfide systems. These Pt-sulfide nanoparticles likely gather during the exsolution of pentlandite from MSS to form microscopic cooperite crystals, as observed in the $PtBi_2$-and $PtAs_2$-saturated 25°C experiments.

In all Pd-saturated systems, Pd mineral phases formed subhedral or rounded grains. All Pd minerals crystallized from immiscible semimetal melt below 750°C; it is hard to conclude whether this happened just below 750°C or at much lower temperatures. The rounded outline of the Pd-semimetal minerals, when included in the ISS, may suggest that they crystallized from trapped melts in the ISS. The single occurrence of merenskyite ($PdTe_2$), which had a subhedral outline in the sulfide melt at 750°C, suggests that it crystallized at temperatures slightly higher than 700°C; the solidus of the sulfide melt (Helmy et al., 2021). The strong semimetal-Pd complexation and the weak chemical affinity between Pd and S (Helmy et al., 2023) explain the absence of any Pd-sulfides in all systems at all temperatures.

The Pd contents in the MSS of the four systems dropped sharply with temperature; the Pd contents were undetectable in pyrrhotite in the 25°C experiment in the four systems. Because Pd does not substitute in MSS as PdS associations (Helmy et al., 2023), the relatively high Pd contents in the MSS of the 950°C runs is probably due to submicron Pd-semimetal melt inclusions in the MSS (e.g., Helmy et al., 2023). These submicron melt inclusions were not

observed in experiments at 25°C, indicating that Pd was redistributed during cooling, leading to the low Pd content in pyrrhotite in the 25°C experiments. This is supported by the common presence of small Pd-semimetal melt grains at the MSS-sulfide melt interface at 750°C (see Figure 8C).

2) How do textures and compositions of the Pt and Pd minerals develop during cooling?

Pentlandite, pyrrhotite, chalcopyrite, and cubanite are the final crystallization products of the sulfide liquid. These base metal phases are the decomposition products of MSS and ISS below 450°C. Helmy et al. (2021) showed that MSS exsolves pentlandite at 450°C to form granular pentlandite at the MSS-ISS contact. The ISS exsolves chalcopyrite, cubanite, and minor pentlandite flames at 250°C. Cubanite decomposes later to pyrrhotite and chalcopyrite. The sulfide textures in the 25°C runs of all the systems are consistent with the observations by Helmy et al. (2021), although the systems are saturated with Pt- and Pd-semimetal components. This indicates that Pt- and Pd-semimetal phases are almost completely immiscible in the sulfide component and do not influence the sulfide phase relations, although their presence may lower the solidus temperatures of the sulfide phases, especially at high temperatures (e.g., Helmy and Botcahrnikov, 2020).

Although most of the grains of the Pt mineral phases are found in the Ccp-Cb matrix at 25°C, they do not show any preference for any of the base metal sulfides. All Pt-phases encapsulated in the MSS are commonly encrusted by pentlandite at 25°C, indicating that the later appearance of pentlandite may isolate Pt-phases from further reactions with the host MSS. The relatively large sizes of Pt mineral grains in the decomposed ISS at 25°C suggest that they grew during cooling before the sulfide melt solidified to ISS. Additionally, there is no chemical change in the Pt mineral phases with cooling. From a textural point of view, it seems that the needle-like crystals of moncheite in the MSS and ISS of the PtTe$_2$-saturated sulfide at 750°C and 25°C are high-temperature phases. Because they show the same orientation in the MSS and ISS (although the MSS and ISS formed at different temperatures), it is possible that these crystals existed earlier in the submicroscopic scale in the MSS and sulfide melt and assembled to larger sizes during cooling (e.g., Helmy et al., 2023). The relatively high Pt and semimetal contents of MSS at 950°C in all systems may support this scenario.

At 950°C, Pd forms immiscible melt droplets in all systems; these melt droplets mainly reside in the sulfide melt, although they could also be trapped in the MSS, consistent with the incompatible behavior of Pd and the semimetals in the MSS-sulfide melt system (Helmy et al., 2007; 2013; Helmy and Botcahrnikov, 2020). With cooling, the melt droplets keep their rounded outline when included in the MSS and become larger when they occur in the sulfide melt. A Ni-sulfarsenide (gersdorffite, NiAsS) crystallized inside the Pd-As melt droplet only at 750°C in the PdAs$_2$-saturated experiment. Below 750°C, the melt droplets keep their rounded outline and crystallize to Pd-semimetal minerals. The small Pd mineral grains observed at the contacts between the MSS and ISS in the four systems are probably the result of the migration of Pd into the sulfide melt before it crystallizes to ISS (Helmy et al., 2023). At

25°C, most Pd mineral grains are concentrated in the decomposed ISS, with no preference for any base metal sulfide. The presence of small Pd-semimetal droplets encapsulated in the MSS at high temperatures and their crystallization to Pd-semimetal minerals at low temperatures probably explains the presence of Pd-semimetal minerals in pyrrhotite and pentlandite in natural ores thought to be exsolved from the MSS, which rarely accommodate Pd.

The compositions of the Pd-semimetal phases (melt and minerals) change with cooling (Table 2). The Cu contents of the immiscible Pd-semimetal melts are higher in the PdTe$_2$- and PdBi$_2$-saturated melts but drop with cooling in the four systems. The high Cu content of the Pd-bismuthinide melt at 950°C is probably due to the incomplete separation of the Pd-bismuthinide melt from the sulfide melt. In agreement with previous studies (Helmy et al., 2007; 2013; Helmy and Botcahrnikov, 2020), the Cu partition coefficient $D_{Cu}^{(telluride\ melt/sulfide\ melt)}$ is higher than that between Pd-arsenide and Pd-antimonide and sulfide melts. The high Ni content of the Pd-semimetal melts (at 950°C and 750°C) and phases (at 25°C) (Table 2) is probably due to equilibration with the host sulfides.

3) Ni-semimetal minerals: when do they form and what is their genetic significance?

Nickel is a major constituent of magmatic, hydrothermal, and metamorphosed sulfide deposits in mafic-ultramafic rocks. Although Ni-semimetal minerals (melonite NiTe$_2$, gersdorfite NiAsS and nisbite, NiSbS) are common in these sulfide deposits (Cabri and Laflamme, 1976; Garuti and Rinaldi, 1986; Helmy et al., 1995; Helmy, 2005), only Ni gersdorfite (NiAsS) appeared in the PdAs$_2$-saturated system at 750°C and 25°C. The Ni content of all Pt minerals is very low; only the Pt-bismuthinide melt at 950°C and the PtBi$_2$ phase at 750°C contain wt.% values of Ni (Table 1). The absence of Ni-arsenides, tellurides, and antimonides in the experiments suggest that the affinity of As, Te, and Sb to combine with Pt is stronger than their affinity to combine with Pd and Ni. The formation of Ni-tellurides and antimonides requires high (Te + Sb)/(Pt + Pd) ratios in the mineralizing fluids, and they form only after Pt and Pd tellurides and antimonides form. Gersdorfite crystallization before palladoarsenide explains the high concentration of Pd in gersdorfite in Cu-Ni-sulfide deposits (e.g., Barkov et al., 1999).

Helmy et al. (2007) stated that melonite (NiTe$_2$) should be expected to form only at high Te/PGE ratios, i.e., after the crystallization of the precious metal PGE tellurides, at which point there is still sufficient Te in the system to stabilize inter-metallic compounds such as Ni. Our starting mixes have Te/Pt and Te/Pd ratios of 2. Because Te has a strong chemical affinity to complex with Pt and Pd (Helmy et al., 2007), all Te is consumed by Pt- and Pd-phases, and the activity of Te is too low to stabilize melonite. In nature, the (Pt + Pd)/(Te + Bi + Sb) ratio is approximately 0.3 (Piña et al., 2008); hence, high activities of Te, Sb, and Bi are likely after the formation of Pt- and Pd-semimetal minerals. The excess semimetals will produce melt droplets down to 750°C (Anenburg and Mavrogenes, 2020), from which Ni tellurides may crystallize. Because Te is highly incompatible in the MSS, it is not likely that melonite will

form by exsolution from the MSS, as suggested by Helmy et al. (2007).

4 Conclusion

The stepped experimental approach we used allowed us to compare the mineralogy, compositions, and textures of Pt- and Pd-semimetal phases at high and low temperatures in the same starting sulfide system. Apart from Pt-bismuthinide, Pt-arsenides, tellurides, and antimonides crystallize directly from the semimetal-saturated sulfide liquid at temperatures >950°C and by assembling submicron crystals from the MSS and ISS at temperatures <450°C. Once formed, these Pt mineral phases keep their composition unchanged during cooling. The decomposition of the MSS and ISS to base metal sulfides at temperatures below 450°C changes the textures of the Pt phases. All Pd-semimetal phases form below 750°C from the immiscible Pd-semimetal melt. The textures of Pt and Pd minerals are controlled by the decomposition process of the MSS and ISS at temperatures below 450°C. Only Ni-arsenide precedes Pd-arsenide in crystallization; it crystallizes directly from the Ni-bearing immiscible Pd-arsenide melt above 750°C. Nickel has a weaker chemical affinity with Te, Sb, and Bi than with As. Although Ni arsenides could form as a late magmatic phase, all other Ni-semimetal minerals are probably low-temperature phases that form when the semimetal/(Pt + Pd) atomic ratio of the system is >2.

Data availability statement

The raw data supporting the conclusion of this article will be made available by the authors, without undue reservation.

Author contributions

HH: Conceptualization, Investigation, Data Curation, Writing–original draft, RB: Writing–review and editing. CB: Writing–review and editing. SB: Writing–review and editing.

Funding

Acknowledgments

Conflict of interest

The authors declare that the research was conducted in the absence of any commercial or financial relationships that could be construed as a potential conflict of interest.

Publisher's note

All claims expressed in this article are solely those of the authors and do not necessarily represent those of their affiliated organizations, or those of the publisher, the editors and the reviewers. Any product that may be evaluated in this article, or claim that may be made by its manufacturer, is not guaranteed or endorsed by the publisher.

References

Anenburg, M., and Mavrogenes, J. (2020). Noble metal nanonugget insolubility in geological sulfide liquids. *Geology* 48, 939–943. doi:10.1130/g47579.1

Bai, L., Barnes, S.-J., and Baker, D. (2017). Sperrylite saturation in magmatic sulfide melts: implications for formation of PGE-bearing arsenides and sulfarsenides. *Am. Mineralogist* 102, 966–974. doi:10.2138/am-2017-5631

Ballhaus, C., and Ryan, C. G. (1995). Platinum-group elements in the Merensky reef. I. PGE in solid solution in base metal sulfides and the down-temperature equilibration history of Merensky ores. *Contributions Mineralogy Petrology* 122, 241–251. doi:10.1007/s004100050124

Barin, I. (1995). Thermochemical data of pure substances I Þ II.

Barkov, A., Thibault, Y., Laajoki, K. V. O., Melezhik, V. A., and Nilsson, L. P. (1999). Zoning and substitutions in Co–Ni–(Fe)–PGE sulfarsenides from the mount general skya layered intrusion, arctic Russia. *Can. Mineral.* 37, 127–142.

Barkov, A. Y., Laflamme, J. H. G., Cabri, L. J., and Martin, R. F. (2002). Platinum-group minerals from the wellgreen ni cu pge deposit, yukon, Canada. *Can. Mineral.* 40, 651–669. doi:10.2113/gscanmin.40.2.651

Barnes, S. J., Fisher, L. A., Godel, B., Pearce, M. A., Maier, W. D., Paterson, D., et al. (2016). Primary cumulus platinum minerals in the Monts de Cristal complex, Gabon, magmatic microenvironments inferred from high-definition X-ray fluorescence microscopy. *Contributions Mineralogy Petrology* 171 (3), 23–18. doi:10.1007/s00410-016-1232-1

Cabri, L. J., and Laflamme, J. H. G. (1976). The mineralogy of the platinum-group elements from some copper–nickel deposits of the Sudbury area, Ontario. *Econ. Geol.* 71, 1159–1195. doi:10.2113/gsecongeo.71.7.1159

Cawthorn, R. G., Lee, C. A., Schouwstra, R. P., and Mellowship, P. (2002). Relationship between PGE and PGM in the Bushveld Complex. *Can Mineral* 40, 311–328.

Daltry, V. D. C., and Wilson, A. H. (1997). Review of platinum-group mineralogy, compositions and elemental associations of the PG-minerals and unidentified PGE-phases. *Mineralogy Petrology* 60, 185–229. doi:10.1007/bf01173709

Dare, S. A. S., Barnes, S.-J., Prichard, H., and Fisher, P. C. (2010). The timing and formation of platinum-group minerals from the Creighton Ni– Cu-platinum-group element sulfide deposit, Sudbury, Canada, early crystallization of PGE-rich sulfarsenides. *Econ. Geol.* 105, 1071–1096. doi:10.2113/econgeo.105.6.1071

Garuti, G., and Rinaldi, R. (1986). Mineralogy of melonite-group and other tellurides from the Ivrea–Verbano basic complex, western Italian Alps. *Econ. Geol.* 81, 1213–1217. doi:10.2113/gsecongeo.81.5.1213

Godel, B., Barnes, S. J., Barnes, S.-J., and Maier, D. (2010). Platinum ore in three dimensions: insights from high-resolution X-ray computed tomography. *Geology* 38 (12), 1127–1130. doi:10.1130/g31265.1

Godel, B., Barnes, S.-J., and Maier, W. D. (2007). Platinum-group elements in sulphide minerals, platinum-group minerals, and whole-rocks of the Merensky reef (bushveld complex, South Africa): implications for the formation of the reef. *J. Petrology* 48, 1569–1604. doi:10.1093/petrology/egm030

Hanley, J. (2007). The role of arsenic-rich melts and mineral phases in the development of high-grade Pt–Pd mineralization within komatiite-associated magmatic Ni–Cu sulfide horizons at Dun-donald Beach South, Abitibi Subprovince, Ontario, Canada. *Econ. Geol.* 102, 305–317. doi:10.2113/gsecongeo.102.2.305

Helmy, H. M. (2005). Melonite-group minerals and other tellurides from three Cu–Ni–PGE prospects, Eastern Desert, Egypt. *Ore Geol. Rev.* 26, 305–324. doi:10.1016/j.oregeorev.2005.04.001

Helmy, H. M., Ballhaus, C., Berndt, J., Bockrath, C., and Wohlgemuth-Ueberwasser, C. (2007). Formation of Pt, Pd and Ni tellurides: experiments in sulfide–telluride systems. *Contributions Mineralogy Petrology* 153, 577–591. doi:10.1007/s00410-006-0163-7

Helmy, H. M., Ballhaus, C., Fonseca, R. O. C., and Nagel, T. J. (2013). Fractionation of platinum, palladium, nickel, and copper in sulfide-arsenide systems at magmatic temperature. *Contributions Mineralogy Petrology* 166, 1725–1737. doi:10.1007/s00410-013-0951-9

Helmy, H. M., Ballhaus, C., Wohlgemuth-Ueberwasser, C., Fonseca, R., and Laurenz, V. (2010). Partitioning of Se, As, Sb, Te and Bi between monosulfide solid solution and sulfide melt – application to magmatic sulfide deposits. *Geochem. Cosmochem. Acta* 74, 6174–6179. doi:10.1016/j.gca.2010.08.009

Helmy, H. M., and Botcharnikov, R. (2020). Experimental determination of the phase relations of Pt and Pd antimonides and bismuthinides in the Fe-Ni-Cu sulfide systems between 1100 and 700°C. *Am. Mineralogist* 105 (3), 344–352. doi:10.2138/am-2020-7154

Helmy, H. M., Botcharnikov, R., Ballhaus, C., Wirth, R., Schreiber, A., and Buhre, S. (2023). How Pt and Pd are hosted in magmatic sulfides, substitutions and/or inclusions? *Contributions Mineralogy Petrology* 178, 41. doi:10.1007/s00410-023-02018-8

Helmy, H. M., Botcharnikov, R., Ballhaus, C., Zemlitskaya, A., Wirth, R., Schreiber, A., et al. (2021). Evolution of magmatic sulfide liquids: how and when base metal sulfides crystallize? *Contributions Mineralogy Petrology* 176 (12), 107–115. doi:10.1007/s00410-021-01868-4

Helmy, H. M., and Bragagni, A. (2017). Platinum-group elements fractionation by selective complexing, the Os, Ir, Ru, Rh-arsenide-sulfide systems above 1020°C. *Geochimica Cosmochimica Acta* 216, 169–183. doi:10.1016/j.gca.2017.01.040

Helmy, H. M., and Fonseca, R. O. C. (2017). The behavior of Pt, Pd, Cu and Ni in the Se-sulfide system between 1050 and 700°C and the role of Se in platinum-group elements fractionation in sulfide melts. *Geochimica Cosmochimica Acta* 216, 141–152. doi:10.1016/j.gca.2017.05.010

Helmy, H. M., Stumpfl, E. F., and Kamel, O. A. (1995). Platinum-group minerals from the metamorphosed abu swayel Cu-Ni-PGE deposit, south eastern desert, Egypt. *Econ. Geol.* 90, 2350–2360. doi:10.2113/gsecongeo.90.8.2350

Holwell, D., and McDonald, I. (2007). Distribution of platinum-group elements in the Platreef at Overysel, northern Bushveld Complex: a combined PGM and LA-ICP-MS study. *Contributions Mineralogy Petrology* 154, 171–190. doi:10.1007/s00410-007-0185-9

Junge, M., Wirth, R., Oberthur, R., Melcher, F., and Schreiber, A. (2014). Mineralogical siting of platinum-group elements in pentlandite from the Bushveld Complex. South Africa. *Miner. Deposista* 50, 41–54. doi:10.1007/s00126-014-0561-0

Magyarosi, Z., Watkinson, D. H., and Jones, P. C. (2002). Mineralogy of Ni-Cu-Platinum-Group element sulfide ore in the 800 and 810 orebodies, copper cliff south mine, and P-T-X conditions during the formation of platinum-group minerals. *Econ. Geol.* 97, 1471–1486. doi:10.2113/gsecongeo.97.7.1471

Maier, W. D., Rasmussen, B., Fletcher, I. R., Godel, B., Barnes, S. J., Fisher, L. A., et al. (2015). Petrogenesis of the ~2·77 Ga monts de Cristal complex, Gabon: evidence for direct precipitation of Pt-arsenides from basaltic magma. *J. Petrol.* 56, 1285–1308. doi:10.1093/petrology/egv035

McDonald, I. (2008). Platinum-group element and sulphide mineralogy in ultramafic complexes at western Andriamena, Madagascar. *Appl. Earth Sci. (Trans. Inst. Min. Metall. Sect. B)* 117, B1–B10. doi:10.1179/174327508x309678

Piña, R., Gervilla, F., Helmy, H. M., Ballhaus, C., and Fonseca, R. (2020). Partition behavior of platinum-group elements during the segregation of arsenide melts from sulfide magma. *Am. Mineralogist* 105, 1889–1897. doi:10.2138/am-2020-7477

Piña, R., Gervilla, F., Ortega, L., and Lunar, R. (2008). Mineralogy and geochemistry of platinum-group elements in the Aguablanca Ni–Cu Deposit (SW Spain). *Mineralogy Petrology* 92, 259–282. doi:10.1007/s00710-007-0195-3

Prichard, H. M., Barnes, S.-J., Maier, W. D., and Fisher, P. C. (2004). Variations in the nature of the platinum-group minerals in a cross-section through the Merensky Reef at Impala Platinum: implications for the mode of formation of the reef. *Canadian Mineralogist* 42, 423–437.

Toulmin, P., and Barton, P. N. (1964). A thermodynamic study of pyrite and pyrrhotite. *Geochimica Cosmochimica Acta* 28, 641–671. doi:10.1016/0016-7037(64)90083-3